



HAL
open science

Local vs global approaches to treat two equivalent methyl internal rotations and ^{14}N nuclear quadrupole coupling of 2,5-dimethylpyrrole

Thuy Nguyen, Wolfgang Stahl, Ha Vinh Lam Nguyen, Isabelle Kleiner

► **To cite this version:**

Thuy Nguyen, Wolfgang Stahl, Ha Vinh Lam Nguyen, Isabelle Kleiner. Local vs global approaches to treat two equivalent methyl internal rotations and ^{14}N nuclear quadrupole coupling of 2,5-dimethylpyrrole. *Journal of Chemical Physics*, 2021, 154 (20), pp.204304. 10.1063/5.0049418 . hal-03254852

HAL Id: hal-03254852

<https://hal.science/hal-03254852>

Submitted on 9 Jun 2021

HAL is a multi-disciplinary open access archive for the deposit and dissemination of scientific research documents, whether they are published or not. The documents may come from teaching and research institutions in France or abroad, or from public or private research centers.

L'archive ouverte pluridisciplinaire **HAL**, est destinée au dépôt et à la diffusion de documents scientifiques de niveau recherche, publiés ou non, émanant des établissements d'enseignement et de recherche français ou étrangers, des laboratoires publics ou privés.

Local versus global approaches to treat two equivalent methyl internal rotations and ^{14}N nuclear quadrupole coupling of 2,5-dimethylpyrrole

Thuy Nguyen^a, Wolfgang Stahl^{b*}, Ha Vinh Lam Nguyen^{a,c**}, Isabelle Kleiner^a

^a Laboratoire Interuniversitaire des Systèmes Atmosphériques (LISA), CNRS UMR 7583, Université Paris-Est Créteil, Université de Paris, Institut Pierre Simon Laplace, 61 avenue du Général de Gaulle, 94010 Créteil cedex, France

^b Institute of Physical Chemistry, RWTH Aachen University, Landoltweg 2, 52074 Aachen, Germany

^c Institut Universitaire de France (IUF), 1 rue Descartes, 75231 Paris cedex 05, France

* Passed away before publication.

** Corresponding author. Email: lam.nguyen@lisa.ipsl.fr

ABSTRACT

The microwave spectrum of 2,5-dimethylpyrrole was recorded using a molecular jet Fourier transform microwave spectrometer operating in the frequency range from 2 to 26.5 GHz. Only one stable conformer was observed as expected and confirmed by quantum chemical calculations carried out to complement the experimental analysis. The two equivalent methyl groups cause each rotational transition to split into four torsional species, which is combined with the quadrupole hyperfine splittings in the same order of magnitude arising from the ^{14}N nucleus. This results in a complicated spectrum feature. The spectral assignment was done separately for each torsional species. Two global fits were carried out using the *XIAM* code and the *BELGI-C_{2v}-2Tops-hyperfine* code, a modified version of the *BELGI-C_{2v}-2Tops* code, giving satisfactory root-mean-square deviations. The potential barriers to internal rotation of the two methyl groups were determined to be $V_3 = 317.208(16) \text{ cm}^{-1}$. The molecular parameters were obtained with high accuracy, providing all necessary ground state information for further investigations in higher frequency ranges and on excited torsional-vibrational states.

I. INTRODUCTION

Besides the classic topics in structural chemistry,¹ large amplitude motions (LAMs), e.g., internal rotation,² ring puckering,³ and inversion motion,⁴ form a very active area in microwave spectroscopy. The effect of a methyl internal rotation on the rotational spectrum is that each rotational transition exhibits a torsional fine structure caused by the interaction of the methyl internal and the overall rotation. This fine structure, consisting of A-E doublets, depends on the height of the potential barrier hindering the internal rotation. If the barrier is very high, the internal motion of the methyl group corresponds to simple harmonic oscillation, whereas if the barrier is very low, the internal motion corresponds to an essentially free rotation.

In the presence of two methyl internal rotors, the fine structure consists of quartets (two equivalent tops) and quintets (two inequivalent tops). Analyzing their microwave spectra is a rather complicated task. Fitting the spectrum with sufficient accuracy often requires effective Hamiltonians to be included in the model. Due to challenges in both spectral assignment and fit, only a limited number of two-top molecules have been investigated, as reviewed by Nguyen and Kleiner.² Unlike inequivalent two-top cases where the point group of the frame symmetry can be C_1 or C_s , in the cases of two equivalent methyl groups, due to the higher molecular symmetry requirement, e.g., C_2 , C_{2h} , or C_{2v} , the number of studies reported in the literature are even smaller. Some examples of equivalent two-top molecules are dimethylgermane,⁵ dimethylamine,⁶ dimethylketene,⁷ isobutylene,⁸ propane,⁹ 2,6-lutidine,^{10,11} difluorodimethylsilane,¹² 2-bromopropane,¹³ dimethyl sulfate,¹⁴ acetone,^{15,16} dimethyl ether,¹⁷ diethyl ketone,¹⁸ dimethyl sulfide,¹⁹ 2,5-dimethylthiophene,²⁰ 2,5-dimethylfuran,²¹ and 2,6-dimethylfluorobenzene.²² The spectral analysis can be challenging in some cases like 2,6-lutidine,^{10,11} that understanding the microwave spectra still remains incomplete. In the present work, we studied the microwave spectrum of 2,5-dimethylpyrrole (25DMP), a nitrogen-containing five-membered ring which contains two equivalent methyl groups and a nitrogen atom with support from quantum chemical calculations. The investigation adds an important contribution to the limited number of studies on two equivalent methyl rotors.

While high barriers result in rather small torsional splittings in the order of a few tens of kHz to a few MHz as found for 4- and 5-methylthiazole,^{23,24} or 2-chloro-4-fluorotoluene,²⁵ in the case of low barriers, the splittings can be up to several GHz,²⁶⁻²⁸ making the spectral assignment difficult. If the molecule contains also a ^{14}N nucleus which causes a quadrupole hyperfine structure with splittings also from a few tens of kHz to 2 MHz in addition, the spectral analysis is even challenging for high barrier cases, since the hyperfine patterns overlap with the torsional splittings.²⁹ To confirm that the assignments are correct, it is often useful to fit each torsional species separately. For 25DMP, we wrote a program called *WSI8* which takes into account the quadrupole coupling of one ^{14}N nucleus for this purpose.

The effects of internal rotation arising from two methyl groups in combination with one weakly coupling ^{14}N quadrupole nucleus can be treated in a global fit with the program *XIAM*.³⁰ However, *XIAM* has its weakness in reproducing the experimental data to measurement accuracy if the torsional barrier is low.³¹⁻³³ It is often discussed that a reason might be the neglect of interactions between different v_t states, but a study on *m*-methylanisole has proven this assumption to be false.³⁴ Recent studies on 4-methylacetophenone,³⁵ 3-fluorotoluene,³⁶ and *m*-methylanisole³⁷ strongly suggest the limited number of parameters available in *XIAM* to be the main reason.

The initial version of the *BELGI-C_s* program³⁸ has been extended to a hyperfine version for one-top, *BELGI-C_s-hyperfine*,³⁹ and recently also for molecules with two inequivalent methyl tops, *BELGI-C_s-2Tops-hyperfine*.³¹ In many cases, the *BELGI* code shows great advantages over *XIAM* in reducing the root-mean-square (rms) deviations.^{26,31,39-41} To treat the microwave spectrum of 25DMP, we modified the *BELGI-C_{2v}-2Tops* code which was used to fit the rotational spectrum of dimethyl sulfide, properly treating molecules containing two equivalent methyl tops with *C_{2v}* molecular symmetry,¹⁹ to *BELGI-C_{2v}-2Tops-hyperfine* to consider the quadrupole coupling of one ¹⁴N nucleus. The results of *BELGI-C_{2v}-2Tops-hyperfine* will be compared with those of *XIAM*.

II. THEORETICAL

A. Quantum chemical calculations

Quantum chemical calculations were performed at the MP2/cc-pVDZ level of theory using the *GAMESS* program.⁴² The obtained rotational constants, the *V₃* term of the methyl torsional potentials, and the ¹⁴N nuclear quadrupole coupling constants (NQCCs) were used as initial values for assigning the spectrum of 25DMP.

Optimizations of the molecular geometry of 25DMP at the MP2/cc-pVDZ level of theory yielded only one stable conformer with the geometry shown in Fig. 1. The dihedral angles $\alpha_1 = \angle(C_3, C_2, C_6, H_{13})$ and $\alpha_2 = \angle(C_4, C_5, C_7, H_{16})$ are 0° at equilibrium. The nuclear coordinates in the principal axis orientation are given in Table S-I in the Supplementary Material. In order to calculate the ¹⁴N NQCCs, the method of Bailey⁴³ was applied as it is known to give very reliable results.^{31,44-46} The electric field gradient at the site of the ¹⁴N nucleus in 25DMP was calculated at the B3PW91/6-311+G(d,p) level using the molecular geometry given in Fig. 1. The calibration factor $eQ/h = 4.599$ MHz/a.u. recommended for conjugated π systems was used.⁴⁴ The resulting quadrupole coupling constants are $\chi_{aa} = 1.3243$, $\chi_{bb} = 1.665$, and $\chi_{cc} = -2.996$ MHz. Due to the *C_{2v}* symmetry of the molecule, all off-diagonal elements are zero.

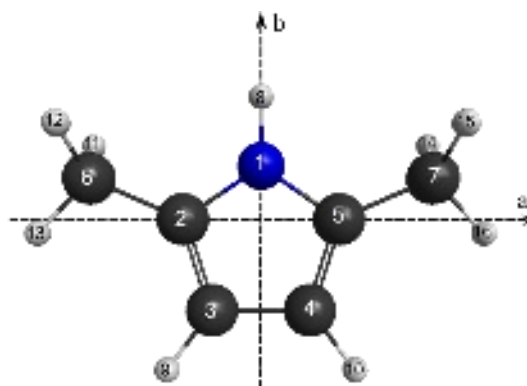


FIG. 1. The molecular geometry of 25DMP calculated at the MP2/cc-pVDZ level of theory. The atom numbering and the principal axis of inertia *a*- and *b*- are given.

A two-dimensional potential energy surface (2D-PES) was calculated at the MP2/cc-pVDZ level by varying the dihedral angles α_1 and $\alpha_2 = \angle(C_4, C_5, C_7, H_{16})$ to predict the barriers to internal rotation and to study the

possible potential coupling effects between the two methyl rotors, as given in Fig. 2. The symmetry adapted Fourier coefficients describing the PES are collected in Table S-II in the Supplementary Material. From the PES, we obtain a V_3 value of 281.9 cm^{-1} for each top with a V_6 contribution of approximately 42.6 cm^{-1} . Moreover, the top-top potential coupling contributes with 10% to the value of the barrier to internal rotation, indicating a weak anti-gearing motion between the two tops, as will be discussed in detail in section IV.C.

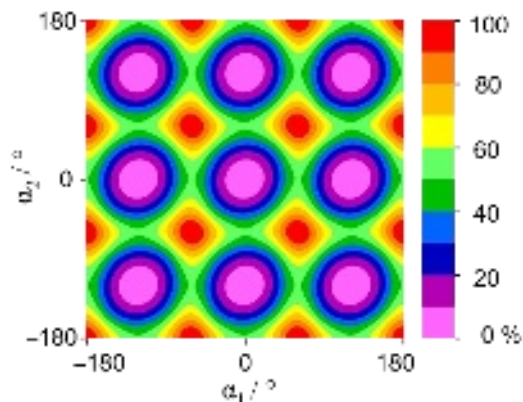


FIG. 2. The potential energy surface of 25DMP calculated at the MP2/cc-pVDZ level of theory obtained by varying the dihedral angles $\alpha_1 = (\text{C}_3, \text{C}_2, \text{C}_6, \text{H}_{13})$ and $\alpha_2 = (\text{C}_4, \text{C}_5, \text{C}_7, \text{H}_{16})$ in a 10° grid, corresponding to the rotations of the methyl groups. The energies (in percent) are color-coded. The global energy minimum is at $E = -287.897702$ Hartree (0 %).

B. Molecular symmetry

In 25DMP, two equivalent methyl groups are attached to a C_{2v} symmetric frame. Its molecular symmetry group is G_{36} with the well-known irreducible representations $A_1, A_2, A_3, A_4, E_1, E_2, E_3, E_4, G$ and the character table given in Table S-III in the Supplementary Material.⁴⁷ In this work, we follow a labeling scheme (00), (01), (11), and (12) which naturally arises from the semi-direct product decomposition $G_{36} = (C_3^I \otimes C_3^I) \ltimes C_{2v}$ as reported by Ezra⁴⁸ and discussed for 2,5-dimethylthiophene by Van *et al.*⁴⁹ but with detailed intuitive interpretation. The label $(\sigma_1, \sigma_2) \cdot X$ of the irreducible representations consists of two parts. The first part arises from the invariant subgroup of G_{36} , which is the direct product $C_3^I \otimes C_3^I$ of the two intrinsic (superscript I) C_3 permutation groups of the internal rotors. Their irreducible representations (σ_1, σ_2) with $\sigma_i = 0, -1, 1$ represent the transformation properties of the C_3 -adapted planar rotor wave functions $e^{i(3k+\sigma)\alpha}$, $k \in Z$ and the torsional angle α , according to the three species A, E_a, E_b of the C_3 group, respectively. For a better readability, we use the number 2 in the symmetry labels for the $\sigma_i = -1$ irreducible representation. Under the C_{2v} frame symmetry, the direct product $C_3^I \otimes C_3^I$ decomposes into four orbits $\{(00)\}, \{(12), (21)\}, \{(11), (22)\},$ and $\{(01), (10), (02), (20)\}$. One representative of each orbit is chosen for the symmetry label. The second part, the label X, is formed by the irreducible representations of the little co-group of a given (σ_1, σ_2) orbit. Here, we will give an intuitive description of this little co-group. The expectation values of the angular momentum of a methyl group are zero for the $\sigma_i = 0$ states. For $\sigma_i = 1$ and -1 states, the angular momenta are non-zero with opposite signs. This can be imagined as no rotation for $\sigma_i = 0$, and a clockwise or a counterclockwise rotation for $\sigma_i = \pm 1$. In the case of the (00) species, none of the tops rotates. There is no displacement of the methyl groups, and in this state the little co-group is C_{2v} with its irreducible representations A_1, B_1, A_2, B_2 . Therefore, we have the G_{36} species (00)· A_1 , (00)· B_1 , (00)· A_2 , (00)· B_2 ,

corresponding to the traditional A_1 , A_2 , A_3 , A_4 labels, respectively. For the (12) orbit, one top rotates clockwise, the other one counterclockwise. Looking at a snapshot at a given time, the point group of the frame symmetry is no longer C_{2v} but C_s symmetry. There is no longer an ab mirror plane but only a bc mirror plane. From the irreducible representations A' and A'' of C_s , we obtain the G_{36} species (12)· A' and (12)· A'' corresponding to E_1 and E_2 , respectively. In the case of the (11) orbit, both tops rotate either clockwise or counterclockwise. Almost all the time, there is no longer any mirror plane in the molecule but the C_2 axis, coinciding with the b axis, remains. The little co-group of the (11) orbit is C_2 with the irreducible representations A and B . We obtain the G_{36} irreducible representations (11)· A and (11)· B , corresponding to E_3 and E_4 . Finally, the (01) orbit describes the case where one top does not rotate and the other one rotates clockwise or counterclockwise. A snapshot of the molecule will not show any non-trivial symmetry elements. The little co-group is C_1 with the species A , and the G_{36} irreducible representation is therefore (01)· A corresponding to G . A comparison of both labeling schemes shows that direct information of the degeneracy of a species, i.e., the non-, double-, and four-fold degeneracy of A , E , G , respectively, is lost. Instead, we obtain intuitive information on the behavior of the internal rotors for a given G_{36} irreducible representation.

25DMP has 9 protons and one ^{14}N nucleus, from which $2^9 \cdot 3 = 1536$ spin functions arise. The selection rules along with the spin statistical weights is given in Table I. In comparison to 2,5-dimethylthiophene,⁴⁹ a factor of 6 was found because the NH group, replacing the sulfur atom in 2,5-dimethylthiophene, adds a proton with two spin states and a ^{14}N nucleus with three spin states while the ^{32}S nucleus has only one spin state. Without taking the spin statistical weights into account, the intensities of all torsional components are the same (see for example Fig. 4 in Ref. ³⁵). When the spin weight was taken into account, the calculated intensities of torsional components are in fairly good agreement with the observed intensities as depicted in Fig. 3. Only for the (12) species, which should be about half as intense as the (00) species, we found that the two lines feature almost the same intensity and have no reasonable explanation for this observation.

Table I: Spin statistical weights of torsional components of allowed transitions of 25DMP

ee \leftrightarrow oo		eo \leftrightarrow oe	
(00)· $A_1 \leftrightarrow$ (00)· A_2	216	(00)· $B_1 \leftrightarrow$ (00)· B_2	168
(12)· $A' \leftrightarrow$ (12)· A''	96	(12)· $A' \leftrightarrow$ (12)· A''	96
(11)· $A \leftrightarrow$ (11)· A	120	(11)· $B \leftrightarrow$ (11)· B	72
(01)· $A \leftrightarrow$ (01)· A	384	(01)· $A \leftrightarrow$ (01)· A	384

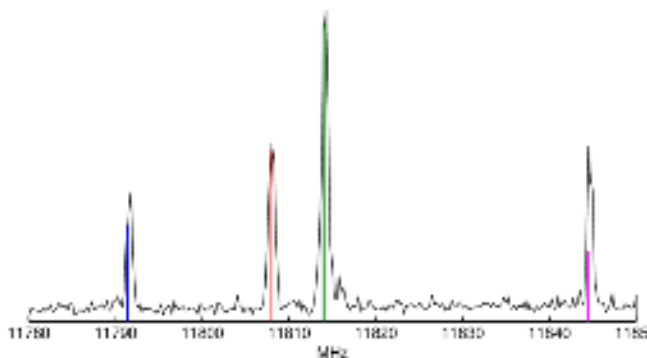


FIG. 3. The broadband scan and the simulated spectrum of the four torsional species (00) in red, (01) in green, (11) in blue, and (12) in purple of the rotational transition $4_{22} \leftarrow 4_{13}$ of 25DMP.

C. The *WSI8* code

The complexity of the spectra of 25DMP caused by two equivalent methyl groups and the presence of a ^{14}N nucleus makes the spectral assignment a challenging task. The splittings of the torsional species for some rotational transitions are within 1 MHz and overlap with the hyperfine splittings of the ^{14}N nucleus. Using a global fit for assignments was very time-consuming and uncertain. From experiences in the literature, separately fitting the torsional species is a good alternative to check the assignments, as successfully done in the investigations in Refs. ^{22,35,50}. To take into account the quadrupole coupling of the ^{14}N nucleus, the *WSI8* code was written. The effective Hamiltonian used in our study is:

$$\mathbf{H} = \mathbf{H}_r + \mathbf{H}_{cd} + \mathbf{H}_{op} + \mathbf{H}_{nq}, \quad (1)$$

with the pure rotational part:

$$\mathbf{H}_r = A\mathbf{P}_z^2 + B\frac{1}{4}(\mathbf{P}_+^2 + \mathbf{P}_-^2 + \mathbf{P}_+\mathbf{P}_- + \mathbf{P}_-\mathbf{P}_+) - C\frac{1}{4}(\mathbf{P}_+^2 + \mathbf{P}_-^2 - \mathbf{P}_+\mathbf{P}_- - \mathbf{P}_-\mathbf{P}_+), \quad (2)$$

the quartic centrifugal distortion terms:

$$\mathbf{H}_{cd} = -\Delta_J\mathbf{P}^4 - \Delta_{JK}\mathbf{P}^2\mathbf{P}_z^2 - \Delta_K\mathbf{P}_z^4 - \delta_J\mathbf{P}^2(\mathbf{P}_+^2 + \mathbf{P}_-^2) - \delta_{K\frac{1}{2}}\{\mathbf{P}_z^2, (\mathbf{P}_+^2 + \mathbf{P}_-^2)\}, \quad (3)$$

the odd-order angular momentum terms:

$$\mathbf{H}_{op} = q\mathbf{P}_z + r\frac{1}{2}(\mathbf{P}_+ + \mathbf{P}_-) + q_J\mathbf{P}^2\mathbf{P}_z + q_K\mathbf{P}_z^3 + \dots, \quad (4)$$

and the nuclear quadrupole coupling Hamiltonian:

$$\mathbf{H}_{nq} = \mathbf{V}^{(2)} \cdot \mathbf{Q}^{(2)}, \quad \chi_{aa} = 2eQV_0^{(2)}, \quad \chi_{bb} - \chi_{cc} = \sqrt{6}eQ(V_2^{(2)} + V_{-2}^{(2)}). \quad (5)$$

The Hamiltonian matrix is set up in the symmetric top basis. Only matrix elements diagonal in J were considered, leading to a matrix size of $(2J+1)(2J+1)$. Both real and complex matrix elements are allowed. The code can be used for fitting microwave spectra of molecules with any point group of the frame symmetry. Effective Hamiltonian terms can be added from the input file in *WSI8*, similar to the *aixPAM* code written for treating the rotational spectrum of one-top molecules.³⁴ These terms are given as a sum of products of the fundamental operator \mathbf{P}^2 , \mathbf{P}_z , the step-up and step-down operators $\mathbf{P}_+ = \mathbf{P}_x + i\mathbf{P}_y$, $\mathbf{P}_- = \mathbf{P}_x - i\mathbf{P}_y$ which are coded as P2, Pz, P+, and P-, respectively. As an example, the operator r_J , multiplying $\frac{1}{2}(\mathbf{P}^2\mathbf{P}_+ + \mathbf{P}^2\mathbf{P}_-)$, is coded as:

$$\begin{aligned} rJ \ 0.5 \ P2 \ P+ \\ rJ \ 0.5 \ P2 \ P- \end{aligned} \quad (6)$$

D. The *BELGI-C_{2v}-2Tops-hyperfine* code

In order to treat the LAMs originating from two methyl groups and a weak nuclear quadrupole coupling caused by a ^{14}N nucleus in the rotational spectrum of 25DMP, the *BELGI-C_{2v}-2Tops* code¹⁹ was modified to *BELGI-C_{2v}-2Tops-hyperfine*. The method is similar to that applied for 4,5-dimethylthiazole.³¹ The only difference is the molecular point group which is C_s in the case of 4,5-dimethylthiazole and C_{2v} in 25DMP.

The Hamiltonian used in *BELGI-C_{2v}-2Tops-hyperfine* is the same as in *BELGI-C_{2v}-2Tops*¹⁹ which is based on the Hamiltonian initially introduced by Ohashi *et al.*⁵⁰ It is written in a slightly modified Principal Axis Method (quasi-PAM). In the Hamilton operator of Eq. (6) from Ref. ⁵⁰ which we also used, the axis system (x, y, z) is chosen in such a way that quadratic cross terms in the angular momentum components \mathbf{P}_x , \mathbf{P}_y , and \mathbf{P}_z are kept fixed to zero at lowest order, which is different from the traditional PAM Hamiltonian with internal rotation (see Eq. (7) of Ref. ⁵⁰). The relations between the parameters of our quasi-PAM and the traditional PAM system are defined in Eqs. (9) to (12) of Ref. ⁵⁰. Unlike in Ref. ⁵⁰, we follow a two-steps diagonalization of the matrix associated to the Hamiltonian. More detailed descriptions are referred to Refs. ¹⁹ and ⁵¹.

The quadrupole energies for each rotational transition in a given torsional state caused by the ¹⁴N nucleus are computed in the *BELGI-C_{2v}-2Tops-hyperfine* code using the perturbation approach where the hyperfine energy expression is

$$E_{hf}(I, J, F) = 2 \frac{f(I, J, F)}{J(J+1)} [\chi_{aa} \langle \mathbf{P}_z^2 \rangle + \chi_{bb} \langle \mathbf{P}_x^2 \rangle - (\chi_{aa} + \chi_{bb}) \langle \mathbf{P}_y^2 \rangle + \chi_{ab} \langle \mathbf{P}_z \mathbf{P}_x + \mathbf{P}_x \mathbf{P}_z \rangle] \quad (7)$$

with the Casimir function $f(I, J, F)$.⁵²

To facilitate the calculations, the numerical expectation values of the quadratic angular momentum components $\langle \mathbf{P}_x^2 \rangle$, $\langle \mathbf{P}_y^2 \rangle$, $\langle \mathbf{P}_z^2 \rangle$, and $\langle \mathbf{P}_z \mathbf{P}_x + \mathbf{P}_x \mathbf{P}_z \rangle$ are quantified and then transferred into Eq. (7). This method allows us to determine the structure of all hyperfine patterns and take the nuclear quadrupole coupling constants into account in a global fit which already treats the internal rotation of two equivalent methyl groups in *BELGI-C_{2v}-2Tops*.¹⁹

III. EXPERIMENTAL

A. Measurements

The rotational spectra of 25DMP were measured with a molecular jet Fourier transform microwave spectrometer operating in the frequency range from 2.0 to 26.5 GHz.⁵³ 25DMP was purchased from TCI Europe, Zwijndrecht, Belgium, with a stated purity of over 97% and was used without any further purification. A small piece of a pipe cleaner containing the substance was put inside a steel tube close to the nozzle. Helium was used as carrier gas and flowed at a backing pressure of approximately 200 kPa over the substance. The mixture of helium and 25DMP was then expanded into the cavity. A broadband scan with a step width of 250 kHz was recorded in the frequency range from 10.6 to 12.5 GHz. Eventually, all spectra were recorded at high resolution where Doppler splittings are observed due to the coaxial arrangement between the molecular beam and the resonators. The measurement accuracy is approximately 4 kHz for all lines.

B. Spectral analysis

Due to the C_{2v} symmetry of 25DMP, we only expected one dipole moment component along the *b* axis which is in agreement with results from quantum chemical calculations stating that $|\mu_a| = 0.00$, $|\mu_b| = 2.10$, and $|\mu_c| = 0.00$ D. Using the calculated rotational constants, *V*₃ potential of the methyl groups, and angles between the principal *a* axis and the internal rotor axes, a spectrum was predicted using the *XIAM* code.³⁰ We first neglected the nuclear

quadrupole hyperfine structure and could identify the four torsional states (00), (01), (11), (12) of some intense transitions such as $2_{12} \leftarrow 1_{01}$, $4_{04} \leftarrow 3_{13}$, and $4_{22} \leftarrow 4_{13}$ by comparing the broadband scan and the predicted spectrum. Using those lines, a fit was carried out, and the fitted molecular parameters enabled us to predict and find further lines in the frequency range of the spectrometer.

The hyperfine structures arising from the nuclear quadrupole coupling of the ^{14}N nucleus were observed for all torsional transitions. The assignment of the hyperfine patterns was first done separately for each torsional species using the *WS18* code. Subsequently, all lines are fitted globally with the programs *XIAM* and *BELGI-C_{2v}-2Tops-hyperfine*. The frequency list along with the residuals obtained with *XIAM*, *BELGI-C_{2v}-2Tops-hyperfine*, and *WS18* are given in Table S-IV in the Supplementary Material.

IV. RESULTS AND DISCUSSION

A. Separate fits

The four torsional species (00), (01), (11), and (12) were fitted separately with the parameters summarized in Table II. All separate fits yielded reasonable standard deviations which are close to the measurement accuracy, showing that all lines are assigned correctly. All geometry parameters in the separate fits are effective and do not present the real geometry of the molecule.

Table II. Molecular parameters of all torsional species of 25DMP obtained from fits with *WS18*.

Par. ^a	Unit	(00)	(01)	(11)	(12)
<i>A</i>	MHz	6294.59598(87)	6291.65826(19)	6288.7238(19)	6288.71917(62)
<i>B</i>	MHz	2016.97245(33)	2016.91615(10)	2016.86103(37)	2016.86032(23)
<i>C</i>	MHz	1557.13464(36)	1557.13473(10)	1557.13585(23)	1557.13595(14)
ΔJ	kHz	0.1258(82)	0.1004(11)	0.1034(41)	0.0991(22)
ΔJK	kHz	-0.152(39)	-0.1723(52)	-0.235(23)	-0.259(13)
ΔK	kHz	5.28(20)	3.913(23)	2.74(41)	2.30(12)
δJ	kHz	0.0521(79)	0.0301(61)	0.0318(50)	0.0285(19)
<i>q</i>	MHz	-	44.94177(36)	-	89.8432(18)
<i>r</i>	MHz	-	6.086(37)	12.311(76)	-
<i>qJ</i>	kHz	-	-1.240(13)	-	-2.588(60)
<i>qK</i>	kHz	-	-41.645(64)	-	-8.452(45)
χ_{aa}	MHz	1.3253(25)	1.3243(15)	1.3262(20)	1.3301(16)
$\chi_{bb} - \chi_{cc}$	MHz	4.6287(49)	4.6339(25)	4.6450(35)	4.6331(29)
N^b		44	98	55	77
σ^c	kHz	4.1	2.5	2.4	2.1

^a All parameters refer to the principal axis system. Watson's *A* reduction and *I* representation were used. Single standard errors in the unit of the last digits are given in parentheses.

^b Number of hyperfine components.

^c Root-mean-square deviation of the fit.

B. Global fits

The microwave spectrum of 25DMP was fitted globally with the programs *XIAM* and *BELGI-C_{2v}-2Tops-hyperfine* with results given in Table III. Both fits give satisfactory rms deviations. In Table III, all parameters are referred to the principal axis system. As the *BELGI-C_{2v}-2Tops-hyperfine* program works in the quasi-PAM system, the

rotational and the quadrupole hyperfine constants need to be converted into the principal axis system for comparison. The complete set of fitted parameters using the *BELGI-C_{2v}-2Tops-hyperfine* code is presented in Table IV.

Table III. Molecular parameters of 25DMP in the principal axis system obtained with *XIAM* (Fit *XIAM*) and *BELGI-C_{2v}-2Tops-hyperfine* (Fit *BELGI*) as well as values calculated at the MP2/cc-pVDZ level of theory. Parameters from the quasi-PAM system are converted into the PAM system using the conversion code introduced in Section 2.3. of Ref. ³¹.

Operator	Par. ^a	Unit	Fit <i>XIAM</i>	Fit <i>BELGI</i> ^b	<i>ab initio</i> ^c
\mathbf{P}_a^2	<i>A</i>	MHz	6290.61862(82)	6290.69(32)	6192.8
\mathbf{P}_b^2	<i>B</i>	MHz	2016.95964(16)	2016.96(17)	1999.7
\mathbf{P}_c^2	<i>C</i>	MHz	1557.07334(14)	1557.06340(11)	1541.2
$-\mathbf{P}^4$	Δ_J	kHz	0.1010(16)		0.0964
$-\mathbf{P}^2\mathbf{P}_a^2$	Δ_{JK}	kHz	-0.2058(96)		-0.2100
$-\mathbf{P}_a^4$	Δ_K	kHz	3.294(39)		3.3804
$-2\mathbf{P}^2(\mathbf{P}_a^2 - \mathbf{P}_c^2)$	δ_J	kHz	0.02840(99)		0.0289
$-\{\mathbf{P}_a^2, (\mathbf{P}_a^2 - \mathbf{P}_c^2)\}$	δ_K	kHz	-		0.0580
	<i>F</i> ₀	GHz	158 ^d	160.238(72) ^e	158
$(\mathbf{p}_{\alpha_1} - \rho\mathbf{P}_a)^2$	<i>F</i>	GHz	164.0340 ^e	164.9605 ^f	
$\{(\mathbf{p}_{\alpha_1} - \bar{\rho}^+\bar{\mathbf{P}}_{r_1}), (\mathbf{p}_{\alpha_2} - \bar{\rho}^+\bar{\mathbf{P}}_{r_2})\}$	<i>F</i> ₁₂	GHz	-5.4211 ^e	-5.74(12) ^e	
$(1/2)(1 - \cos(3\alpha))$	<i>V</i> ₃	cm ⁻¹	317.208(16)	317.9205(41)	281.9
$F\mathbf{P}_a\mathbf{p}_{\alpha_1}$	ρ		0.0370 ^e	0.036460(18) ^e	
$\{(\mathbf{p}_{\alpha_1} - \bar{\rho}^+\bar{\mathbf{P}}_{r_1}), \mathbf{P}_a^2\}$	<i>D</i> _{pi2K}	MHz	0.6996(89)		
	χ_{aa}	MHz	1.3272(21)	1.3267(14)	1.3243
	$\chi_{bb} - \chi_{cc}$	MHz	4.6390(36)	4.6388(31)	4.6610
	$\angle(i_1, a)^g$	°	157.130(22)	156.955(24) ^e	156.41
	$\angle(i_1, b)$	°	67.123(22)	66.955(24) ^e	66.42
	$\angle(i_2, a)^g$	°	22.888(22)	23.045(24) ^e	23.59
	$\angle(i_2, b)$	°	67.112(22)	113.045(24) ^e	66.42
	<i>N</i> _q ^h		274	274	
	<i>rms</i> ^k	kHz	4.8	3.4	

^a All parameters refer to the principal axis system. Watson's A reduction and *F* representation were used.

^b Rotational and quadrupole hyperfine constants obtained by transformation from the quasi-PAM to the PAM system.

^c Calculated at the MP2/cc-pVDZ level. The centrifugal distortion constants were obtained by harmonic frequency calculations.

^d Fixed to the calculated value.

^e Derived parameter in *XIAM*. For *BELGI-C_{2v}-2Tops-hyperfine*, the fitted parameters are $q_1 (= q_2)$ which multiplies the operator $\mathbf{P}_2\mathbf{p}_{\alpha_1}$ (see Table IV). The value of the ρ parameter can be obtained from $q_1 = q_2 = -2F_1\rho_{1z}$ and $r_1 = -r_2 = -2F_1\rho_{1x}$. f_{12} is a floated parameter, with the relation $f_{12} = -2F_{12}$ (see text).

^f Fixed value. In *BELGI-C_{2v}-2Tops-hyperfine*, F_1 (or f_1 in the notation of Ref. ⁵⁰) = F_2 (or f_2), multiplying the operators $\mathbf{p}_{\alpha_1}^2 = \mathbf{p}_{\alpha_2}^2$.

^g $\angle(i, c) = 90^\circ$ for both rotors due to symmetry.

^h Number of hyperfine components.

^k Root-mean-square deviation of the fit.

Table IV. Spectroscopic constants of 25DMP in quasi-PAM obtained with the program *BELGI-C_{2v}-2Tops-hyperfine*.

Operator ^a	Par. ^b	Unit	Value
\mathbf{P}_z^2	<i>A</i>	MHz	6736.22(17)
\mathbf{P}_x^2	<i>B</i>	MHz	2024.689(11)
\mathbf{P}_y^2	<i>C</i>	MHz	1557.06340(11)
$-\mathbf{P}^4$	Δ_J	kHz	0.0392(17)
$-\mathbf{P}_z^4$	Δ_K	kHz	3.433(28)
$-\mathbf{P}^2\mathbf{P}_z^2$	Δ_{JK}	kHz	-0.1561(69)
$\mathbf{p}_1^2 = \mathbf{p}_2^2$	$F_1 = F_2$	GHz	164.9605 ^c
$\mathbf{p}_1\mathbf{p}_2$	f_{12}	GHz	11.47(12)
$(1/2)(1-\cos(3\alpha_1))$	$V_{3,1}$	cm ⁻¹	317.9205(41)
$\mathbf{P}_z\mathbf{p}_1$	q_1	GHz	-12.3329(45)
$\mathbf{P}_x\mathbf{p}_1$	r_1	GHz	-1.5691(12)
$\mathbf{P}_x\mathbf{p}_1\mathbf{P}^2$	r_{1J}	MHz	-11.91(28)
	$2\chi_{aa}$	MHz	2.6533(29)
	$2\chi_{bb}$	MHz	3.3121(27)
	$2\chi_{cc}$	MHz	-5.9654(29)
	N_q^d		274
	rms^e	kHz	3.4

^a All parameters refer to the quasi-PAM system. \mathbf{P}_x , \mathbf{P}_y , \mathbf{P}_z are the components of the overall rotation angular momentum, \mathbf{p}_1 and \mathbf{p}_2 are the angular momentum of the first and the second top, and α_i is the internal rotation angle.

^b Notation used in the input and output. The relations between the parameters of top 1 and top 2 are: $V_{32} = V_{31}$, $V_{32J} = V_{31J}$, $q_1 = q_2$, $r_2 = -r_1$, $r_{2J} = -r_{1J}$.

^c Fixed values.

^d Number of hyperfine components.

^e Root-mean-square deviation of the fit.

C. Discussion

The different approaches used in the *XIAM* and *BELGI-C_{2v}-2Tops-hyperfine* codes lead to different values of fitted parameters which are given in Table III and Table IV, respectively. The rotational constants obtained from the *BELGI-C_{2v}-2Tops-hyperfine* fit, after converting them to the principal axis system, agree well with those obtained from the *XIAM* program. The small deviations are probably not only due to different terms included in the two fits carried out in different coordinate systems but also due to the conversion process. The values of the calculated rotational constants *A*, *B*, *C* deviate by -1.6%, -0.86%, -1.02%, respectively, to the experimental ones obtained with *XIAM*. Since the rotational constants obtained from *ab initio* calculations are evaluated at equilibrium geometry and the experimental constants refer to the vibrational ground state, an agreement better than 1% is hardly feasible. In the *XIAM* fit, four centrifugal distortion constants (except δ_K) are accurately determined while only three of them (Δ_J , Δ_K , Δ_{JK}) are needed to model the microwave spectra of 25DMP with *BELGI*. The calculated values of centrifugal distortion constants are in very good agreement with the experimental ones (see Table III).

To predict the V_3 potential and determine the contributions of higher order terms such as V_6 , V_9 , etc. in the Fourier expansion of the potential function, as well as to study the potential coupling between the methyl groups, three different sets of symmetry adapted terms were used to parameterize the potential functions. For comparison, the contour plots drawn with the Fourier coefficients obtained from those three different

parameterizations are given in Fig. 4. Due to symmetry, only a portion of each PES with the dihedral angles α_1 and α_2 ranging from -60° to 60° is necessary.

The PES (a) in Fig. 4 is obtained after fitting the data points with a constant term and the Fourier term ($\cos(3\alpha_1) + \cos(3\alpha_2)$), with which all data points can be reproduced with a maximum deviation of 10% within the dynamic range. If we included in addition the Fourier terms ($\cos(6\alpha_1) + \cos(6\alpha_2)$) and ($\cos(9\alpha_1) + \cos(9\alpha_2)$), associating with V_6 and V_9 , respectively, as illustrated in the PES (b), the maximum deviation decreased to 2.8 %, and the minimum in (b) is significantly broader than that in (a). The PES (c) represents one unit cell of the PES given in Fig. 2 where also potential coupling terms between the methyl groups are taken into account and the maximum deviation is 1.13%. The potential minimum is slightly distorted along the anti-diagonal which can be interpreted as an anti-gearing motion of the methyl groups close to the minimum. The V_6 and V_9 contributions are approximately 15% and 3%. Experimental information on these contributions cannot be obtained from our spectrum containing only vibrational ground state rotational transitions, which only yields an effective V_3 barrier for both rotors. The *ab initio* results show that the coupling between the two methyl groups is rather weak with contributions of 1.8% and 11% for V_{cc} and V_{ss} , respectively. This is in agreement with our experimental finding that potential coupling terms were not needed in the fits. Details of symmetry adapted terms and their values are given in Table S-II in the Supplementary Material.

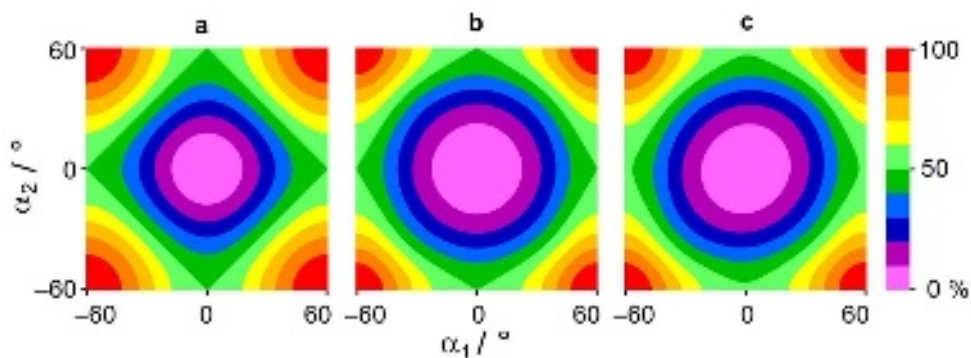


FIG. 4. The PES of 25DMP calculated at the MP2/cc-pVDZ level parameterized using three different sets of symmetry adapted terms. (a) Only the Fourier term ($\cos(3\alpha_1) + \cos(3\alpha_2)$) was used; (b) The Fourier terms ($\cos(6\alpha_1) + \cos(6\alpha_2)$) and ($\cos(9\alpha_1) + \cos(9\alpha_2)$) are included in addition; (c) Potential coupling terms between the methyl groups are also taken into account.

The values of V_3 are determined to be 317.208(16) and 317.9205(41) cm^{-1} with *XIAM* and *BELGI*, respectively. They are in fairly well agreement but not within their error. Qualitatively speaking, the V_3 value should not depend on the axis system (PAM or quasi-PAM) in use. Nevertheless, it depends on different sets of parameters floated in the fit, causing the slight difference between *XIAM* and *BELGI*.

The V_3 potential calculated at the MP2/cc-pVDZ level of theory is 11.2% lower than the observed value, thus giving only the correct order of magnitude. While comparing the value of the V_3 potential obtained for 25DMP with that of 2-methylpyrrole⁴⁶ and those of other five-membered rings, as given in Fig. 5, we found that for 2- and 2,5-methylated heterocyclic rings, the barrier to internal rotation is lowest in mono-methylated and di-methylated thiophenes (1, 2), higher in substituted pyrroles (3, 4), and highest in substituted furans (5, 6). The same holds true when comparing mono-methylated thiazoles, imidazoles, and oxazoles.⁵⁶ We also observe that the barrier is always

larger in dimethylated heterocycles compared to the monomethylated ones. The lower the barrier, the more pronounced this effect.

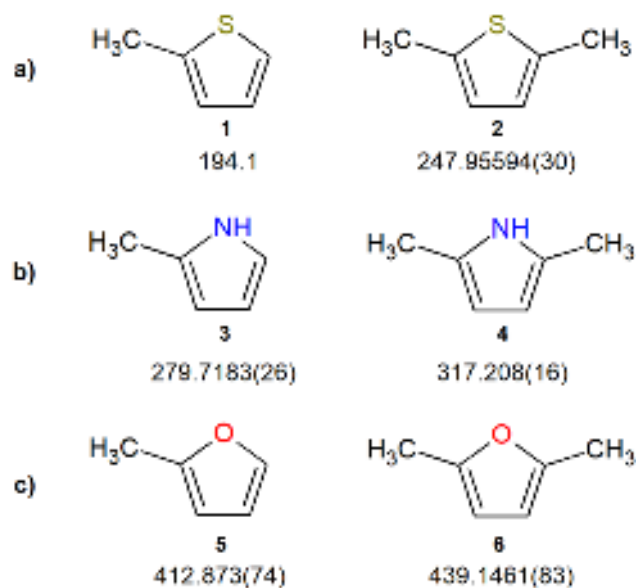


FIG. 5. Comparison of the barriers to internal rotation (in cm⁻¹) of a) 2-methylthiophene (**1**)⁵⁴ and 2,5-dimethylthiophene (**2**),⁴⁹ b) 2-methylpyrrole (**3**)⁴⁶ and 2,5-dimethylpyrrole (**4**, this study), and c) 2-methylfuran (**5**)⁵⁵ and 2,5-dimethylfuran (**6**).²¹ For 2-methylthiophene, the uncertainty was not given in Ref. ⁵⁴.

It should be noted that the correlation between the potential barrier V_3 and $\angle(i,a)$ is -1.000 , showing that if the barrier of V_3 increases, the value of $\angle(i,a)$ will decrease simultaneously. In the *BELGI* approach, the angle $\angle(i,a)$ is not available as a floatable parameter directly but we observed a correlation between V_3 and $F_1 = F_2$. This problem has been solved in previous studies by fixing the values of F_1 and F_2 to those derived from the *XIAM* fit.²⁰ However, in the case of 25DMP, the fit did not converge, and a slight change in F leads to a large different in V_3 even though the rms remains the same. We then tried several values of F starting from the value derived with *XIAM* in steps of 0.05. The value of $F_1 = F_2$ finally chosen yielded a nicely converged fit.

The *XIAM* code is based on the rigid top-rigid frame model in which parameters related with the molecular geometry such as $\angle(i,a)$, $\angle(i,b)$, and F_{12} are available as derived parameters. F_{12} can be floated but it is not recommended since it would lead to the distortion of the molecule. In contrast, the *BELGI* program employed a different approach in which the angles $\angle(i,a)$, $\angle(i,b)$ are not directly involved. Instead, several parameters related to those angles (q_1 , r_1 , f_{12}) can be floated, as for the two-inequivalent-top Hamiltonian introduced by Ohashi *et al.*⁵⁰ As given in the footnote of Table III, $F_1 = F_2$ was kept fixed, and the constants q_1 and r_1 are floated. It is clear in Table IV from the operators they multiply that q_1 and r_1 are essentially $-2F_1\rho_{1a}$ and $-2F_1\rho_{1b}$,⁵¹ respectively, with similar definitions for top 2. In the present study for two equivalent tops, the following parameters were set to be equal:

$$F_1 = F_2; V_{3,1} = V_{3,2}; q_1 = q_2. \quad (8)$$

To be consistent with the convention used in Jabri *et al.*,¹⁹ r_2 was set to be equal but with opposite sign to r_1 :

$$r_2 = -r_1. \quad (9)$$

The magnitude and the signs of those parameters can be derived from equations (11) of Ref. ⁵⁰. It should be noted that the angle θ about the y axis relating the a , b , c principal axes to the x , y , z rho-axes is zero in the case of two equivalent tops. Due to this choice of sign from $r_2 = -r_1$, we also have the relation $f_{12} = -2F_{12}$.

In our previous study on 2-methylpyrrole, the methylation effect arising from one methyl group attached to the pyrrole ring on NQCCs was found to be negligible.⁴⁶ In the present study, two methyl groups with similar functionalities are involved, raising an interesting question whether they possess more significant influence than that of one methyl group. Since the coupling constants obtained in the principal axes of inertia cannot be used directly for comparison, we attempt to compare their values in the principal axes of the field gradient at the nitrogen nucleus in each molecule. For molecules having a plane of symmetry, the principal axis of inertia and a principal axis of the field gradient are collinear with the axis perpendicular to the plane. Assuming that the c axis of the inertial moment coincides with the principal axis y of the field gradient, then the nuclear quadrupole coupling constants in the inertia χ_{aa} , χ_{bb} and those in the field gradient χ_{xx} , χ_{zz} are related by the expression:

$$\begin{pmatrix} \chi_{aa} \\ \chi_{bb} \end{pmatrix} = \begin{pmatrix} \sin^2\theta_{za} & \cos^2\theta_{za} \\ \cos^2\theta_{za} & \sin^2\theta_{za} \end{pmatrix} \cdot \begin{pmatrix} \chi_{xx} \\ \chi_{zz} \end{pmatrix} \quad (10)$$

where θ_{za} is the angle between the z -axis and the a -axis, as illustrated in Fig. 6.

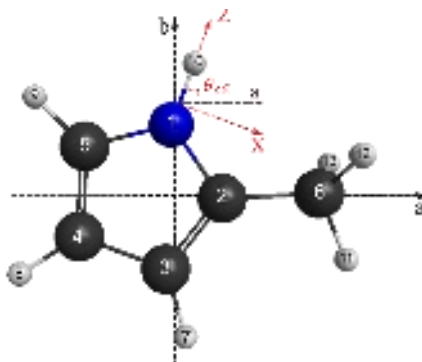


FIG. 6. The principal axes of inertia of the molecule and the principal axes of the field gradient at the nitrogen atom of 2-methylpyrrole.⁴⁶

Because 25DMP has C_{2v} symmetry, the principal axes of the field gradient at the nitrogen nucleus are the same as the principal axes of inertia. Therefore, $\theta_{za} = 0^\circ$, $\chi_{xx} = \chi_{aa} = 1.3272$ MHz and $\chi_{zz} = \chi_{bb} = 1.6559$ MHz. For 2-methylpyrrole,⁴⁶ using the experimentally deduced nuclear quadrupole constants $\chi_{aa} = 1.3345$ MHz and $\chi_{bb} = 1.5127$ MHz together with the calculated value of $\chi_{ab} = 0.0908$ MHz, the angle θ_{za} is determined to be 81.4° . Consequently, χ_{xx} and χ_{zz} are 1.2964 MHz and 1.5508 MHz, respectively. Since the two molecules both have a plane symmetry, the $\chi_{yy} = \chi_{cc}$ and χ_{yy} values are -2.9831 MHz and -2.8472 MHz for 25DMP and 2-methylpyrrole,⁴⁶ respectively. The results show that the second methyl group adjoining to the nitrogen atom in 25DMP increase the NQCC values, especially χ_{zz} , of the nitrogen atom. Nevertheless, the effect of methylations on the pyrrole ring is still negligible, confirming the results found in Ref. ⁴⁶.

V. CONCLUSION

The microwave spectrum of 25DMP with four torsional species arising from two equivalent methyl internal rotations in combination with the presence of quadrupole hyperfine structures originating from a ^{14}N nucleus was recorded under molecular jet conditions and successfully assigned with support of quantum chemical calculations. The *WS18* code, a local approach where the different torsional species were fitted separately, enables us to verify the correctness of the assignment. The *BELGI-C_{2v}-2Tops-hyperfine* version of the *BELGI* code and the program *XIAM* offer a proper tool for a global fit of molecules featuring a C_{2v} symmetry and a weakly coupling quadrupole nucleus, yielding highly accurate molecular parameters and NQCCs. Comparing 25DMP with the mono-methylated derivative 2-methylpyrrole, we conclude that the second methyl group adjoining to the nitrogen atom in 25DMP does not significantly change the field gradient around the nitrogen atom, but slightly increases the NQCC values.

SUPPLEMENTARY MATERIAL

See supplementary information for Cartesian coordinates, coefficients of the PESs, G_{36} character table with the adapted spin weight for 25DMP, and frequency list.

DATA AVAILABILITY STATEMENT

The data that supports the findings of this study are available within the article and its supplementary material.

ACKNOWLEDGMENTS

T.N. thanks the Université de Paris for a Ph.D. fellowship. This work is supported by the Agence Nationale de la Recherche ANR (project ID ANR-18-CE29-0011) and partly supported by the Programme National Physique et Chimie du Milieu Intestellaire (PCMI) of CNRS/INSU with INC/INP co-funded by CEA and CNES.

REFERENCES

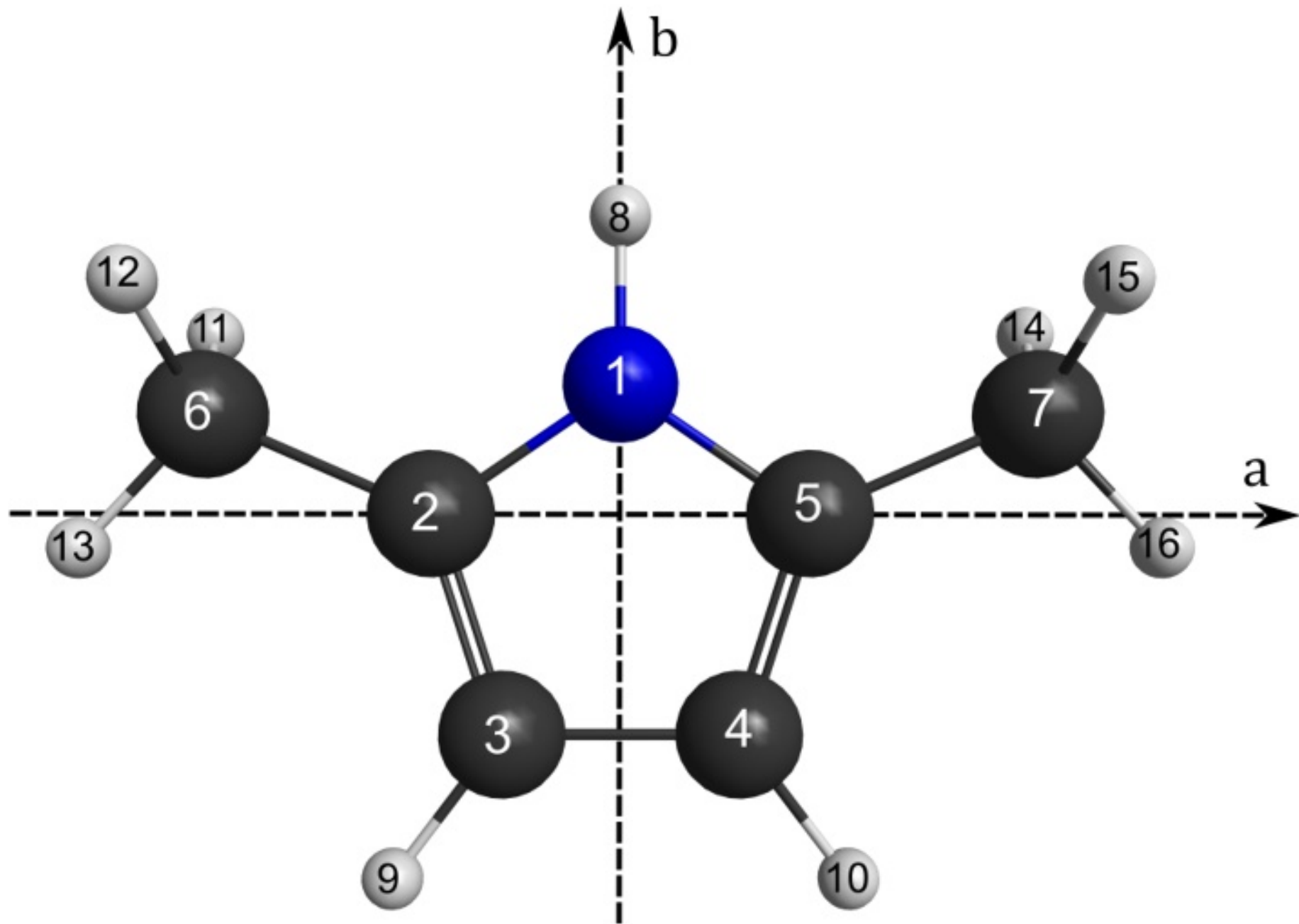
- ¹D. G. Lister, J. N. MacDonald, and N. L. Owen, *Internal Rotation and Inversion: An Introduction to Large Amplitude Motions in Molecules*, Academic Press, New York (1978).
- ²H.V.L. Nguyen, I. Kleiner, Phys. Sci. Rev. (2021), DOI: 10.1515/psr-2020-0037, in press.
- ³A. Legon, Chem. Rev. **80**, 231 (1980).
- ⁴H.V.L. Nguyen, I. Gulaczyk, M. Kręglewski, I. Kleiner, Coord. Chem. Rev. **436**, 213797 (2021).
- ⁵E.C. Thomas, V.W. Laurie, J. Chem. Phys. **50**, 8 (1969).
- ⁶J.E. Wollrab, V.W. Laurie, J. Chem. Phys. **54**, 532 (1971).
- ⁷K.P.R. Nair, H.D. Rudolph, H. Dreizler, J. Mol. Spectrosc. **48**, 571 (1973).

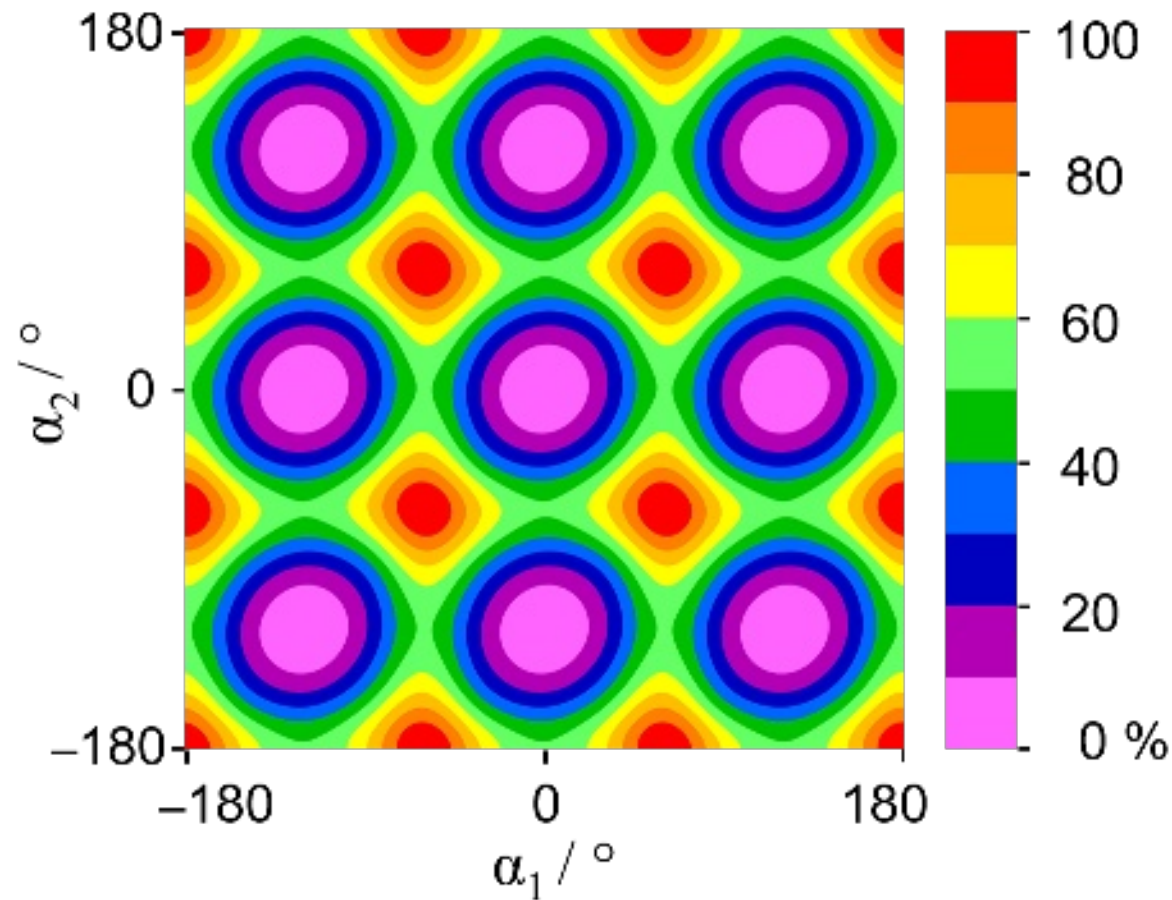
- ⁸H.S. Gutowsky, T.C. Germann, *J. Mol. Spectrosc* **147**, 91 (1991).
- ⁹G. Bestmann, W. Lalowski, H. Dreizler, *Z. Naturforsch.* **40a**, 271 (1985).
- ¹⁰W. Caminati, S.D. Bernardo, *Chem. Phys. Lett.* **171**, 1 (1990).
- ¹¹C. Thomsen, H. Dreizler, *Z. Naturforsch.* **48a**, 1093 (1993).
- ¹²M. Schnell, J.-U. Grabow, H. Hartwig, N. Heineking, M. Meyer, W. Stahl, W. Caminati, *J. Mol. Spectrosc.* **229**, 1 (2005).
- ¹³M. Meyer, W. Stahl, H. Dreizler, *J. Mol. Spectrosc.* **151**, 243 (1992).
- ¹⁴L.B. Favero, L. Evangelisti, G. Feng, L. Spada, W. Caminati, *Chem. Phys. Lett.* **517**, 139 (2011).
- ¹⁵P. Groner, S. Albert, E. Herbst, F. C. De Lucia, F. J. Lovas, B. J. Drouin, J. C. Pearson, *Astrophys. J.* **142**, 145 (2002).
- ¹⁶V.V. Ilyushin, J.T. Hougen, *J. Mol. Spectrosc.* **289**, 41 (2013).
- ¹⁷W. Neustock, A. Guarnieri, J. Demaison, G. Wlodarczak, *Z. Naturforsch.* **45a**, 702 (1990).
- ¹⁸H. V. L. Nguyen, W. Stahl, *ChemPhysChem* **12**, 1900 (2011).
- ¹⁹A. Jabri, V. Van, H. V. L. Nguyen, H. Mouhib, F. Kwabia-Tchana, L. Manceron, W. Stahl, I. Kleiner, *Astron. Astrophys.* **A127**, 589 (2016).
- ²⁰V. Van, W. Stahl, H. V. L. Nguyen, *Phys. Chem. Chem. Phys.* **17**, 32111 (2015).
- ²¹V. Van, J. Bruckhuisen, W. Stahl, V. Ilyushin, H. V. L. Nguyen, *J. Mol. Spectrosc.* **343**, 121 (2018).
- ²²S. Khemissi, H.V.L. Nguyen, *ChemPhysChem* **21**, 1682-1687 (2020).
- ²³W. Jäger, H. Mäder, *Z. Naturforsch.* **42a**, 1405 (1987).
- ²⁴W. Jäger, H. Mäder, *J. Mol. Struct.* **190**, 295 (1988).
- ²⁵K.P.R. Nair, S. Herbers, W.C. Bailey, D.A. Obenchain, A. Lesarri, J.-U. Grabow, H.V.L. Nguyen, *Spectro. Chim. Acta A* **247**, 119120 (2021).
- ²⁶T. Nguyen, V. Van, C. Gutlé, W. Stahl, M. Schwell, I. Kleiner, H.V.L. Nguyen, *J. Chem. Phys.* **152**, 134306 (2020).
- ²⁷L. Ferres, W. Stahl, H.V.L. Nguyen, *J. Chem. Phys.* **151**, 104310 (2019).
- ²⁸R. Kannengießer, M.J. Lach, W. Stahl, H.V.L. Nguyen, *ChemPhysChem* **16**, 1906 (2015).
- ²⁹A. Roucou, M. Goubet, I. Kleiner, S. Bteich, A. Cuisset, *ChemPhysChem* **17**, 2523 (2020).
- ³⁰H. Hartwig, H. Dreizler, *Z. Naturforsch.* **51a**, 923 (1996).
- ³¹V. Van, T. Nguyen, W. Stahl, H. V. L. Nguyen, I. Kleiner, *J. Mol. Struct.* **1207**, 127787 (2020).
- ³²L. Ferres, W. Stahl, I. Kleiner, H.V.L. Nguyen, *J. Mol. Spectrosc.* **343**, 44 (2018).
- ³³H.V.L. Nguyen and W. Stahl, *J. Mol. Spectrosc.* **264**, 120 (2010).
- ³⁴L. Ferres, W. Stahl, H.V.L. Nguyen, *J. Chem. Phys.* **148**, 124304 (2018).

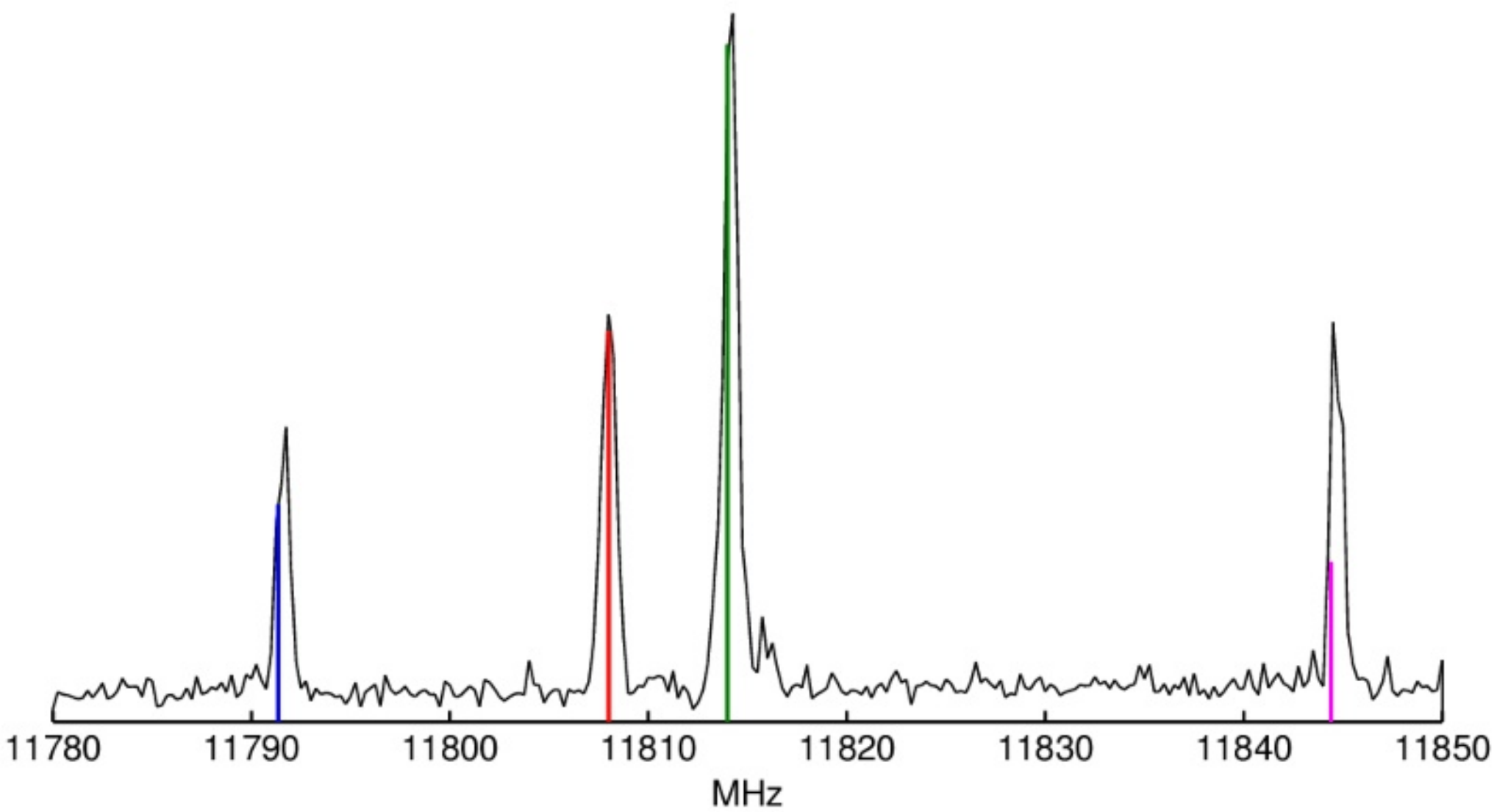
This is the author's peer reviewed, accepted manuscript. However, the online version of record will be different from this version once it has been copyedited and typeset.

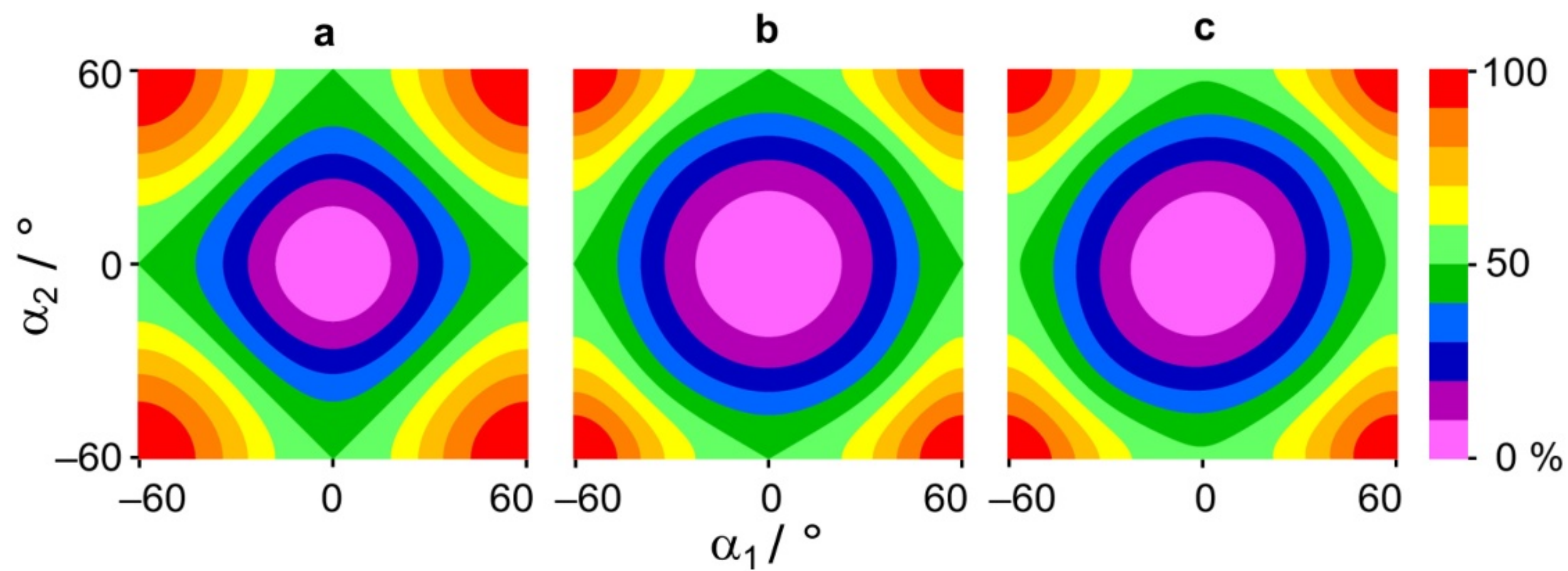
PLEASE CITE THIS ARTICLE AS DOI:10.1063/1.50049418

- ³⁵S. Herbers, S.M. Fritz, P. Mishra, H.V.L. Nguyen, T.S. Zwier, *J. Chem. Phys.* **152**, 074301 (2020).
- ³⁶K.P.R. Nair, S. Herbers, H.V.L. Nguyen, J.-U. Grabow, *Spectro. Chim. Acta A* **242**, 118709 (2020).
- ³⁷S. Herbers, H.V.L. Nguyen, *J. Mol. Spectrosc.* **370**, 111289 (2020).
- ³⁸J. T. Hougen, I. Kleiner and M. Godefroid, *J. Mol. Spectrosc.* **163**, 559 (1994).
- ³⁹R. Kannengießer, W. Stahl, H.V.L. Nguyen, I. Kleiner, *J. Phys. Chem. A* **120**, 3992 (2016).
- ⁴⁰K. Eibl, R. Kannengießer, W. Stahl, H.V.L. Nguyen, I. Kleiner, *Mol. Phys.* **114**, 3483 (2016).
- ⁴¹K. Eibl, W. Stahl, I. Kleiner, H.V.L. Nguyen, *J. Chem. Phys.* **149**, 144306 (2018).
- ⁴²M.W. Schmidt, K.K. Baldrige, J.A. Boatz, S.T. Elbert, M.S. Gordon, J.H. Jensen, S. Koseki, N. Matsunaga, K.A. Nguyen, S.J. Su, T.L. Windus, M. Dupuis, J.A. Montgomery, *J. Comput. Chem.* **14**, 1347 (1993).
- ⁴³W.C. Bailey, *Chem. Phys.* **252**, 57 (2000).
- ⁴⁴R. Kannengießer, W. Stahl, H.V.L. Nguyen, W.C. Bailey, *J. Mol. Spectrosc.* **317**, 50 (2015).
- ⁴⁵J. B. Graneek, W. C. Bailey, M. Schnell, *Phys. Chem. Chem. Phys.* **20**, 22210 (2018).
- ⁴⁶T. Nguyen, C. Dindic, W. Stahl, H. V. L. Nguyen, I. Kleiner, *Mol. Phys.* **118** 1668572 (2020).
- ⁴⁷P. R. Bunker and P. Jensen, *Molecular Symmetry and Spectroscopy*, NRC Research Press, Ottawa, Ontario, Canada (2006).
- ⁴⁸G. S. Ezra, *Symmetry Properties of Molecules, Lecture Notes in Chemistry* 28, Springer-Verlag, Berlin, Heidelberg, New York (1982).
- ⁴⁹V. Van, W. Stahl, H.V.L. Nguyen, *Phys. Chem. Chem. Phys.* **17**, 32111 (2015).
- ⁵⁰N. Ohashi, J.T. Hougen, R.D. Suenram, F.J. Lovas, Y. Kawashima, M. Fujitake, J. Pykad, *J. Mol. Spectrosc.* **227**, 28 (2004).
- ⁵¹M. Tudorie, I. Kleiner, J.T. Hougen, S. Melandri, L.W. Sutikdja, W. Stahl, *J. Mol. Spectrosc.* **269**, 211 (2011).
- ⁵²H.B. G. Casimir, *Teyler's Tweede Genootschap*, E. F. Bohn, Harlem (1936).
- ⁵³J.-U. Grabow, W. Stahl, H. Dreizler, *Rev. Sci. Instrum.* **67**, 4072 (1996).
- ⁵⁴N. M. Pozdeev, L. N. Gunderova, A. A. Shapkin, *Opt. Spektrosk.* **28**, 254 (1970).
- ⁵⁵I. A. Finneran, S. T. Shipman, S. L. Widicus Weaver, *J. Mol. Spectrosc.* **280**, 27 (2012).
- ⁵⁶T. Nguyen, W. Stahl, H.V.L. Nguyen, I. Kleiner, *J. Mol. Spectrosc.* **372**, 111351 (2020).

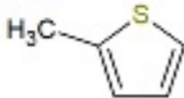






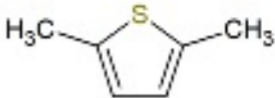


a)



1

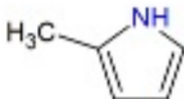
194.1



2

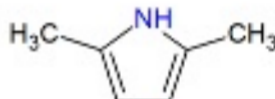
247.95594(30)

b)



3

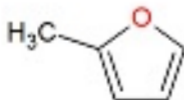
279.7183(26)



4

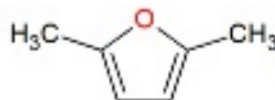
317.208(16)

c)



5

412.873(74)



6

439.1461(83)

